Journal of Applied Polymer Science

Solid-state foaming of isotactic polypropylene and its composites with spherical or fibrous poly(butylenes terephthalate)

Yiwei Luo,[1] Chunling Xin,[1,2] Zhaoping Yang,[1] Baorui Yan,[1] Zhongpeng Li,[1] Xiaohu Li,[1] Yadong He[1,2]

[1]Department of mechanical engineering, College of Mechanical and Electrical Engineering, Beijing University of Chemical Technology, Beijing 100029, China

[2]Engineering Research Center for Polymer Processing Equipment, Ministry of Education, Beijing 100029, China

Correspondence to: Y. He (E-mail: heyd@mail.buct.edu.cn)

ABSTRACT: In this article, the foaming behavior of isotactic polypropylene (iPP) and its composites with spherical or fibrous poly(butylenes terephthalate) (PBT) using supercritical CO_2 as a blowing agent were investigated. Their foaming performances were also compared in relation to the crystal morphology and rheological behavior of PP. Results demonstrate that crystal structures significantly impacted the cell structures of foams. At relatively low temperature, microcells appeared at the centers of PP spherulites where the melting started. Particularly, bi-modal cell structure formed in the foamed PP with increasing temperature. However, in the foamed PP composites with spherical or fibrous PBT, this structure almost disappeared due to the smaller PP spherulites. In foaming PP/PBT composites, the heterogeneous nucleation of spherical or fibrous PBT was effective at reducing cell size as well as improving cell density and cell uniformity. The fibrous PBT also acted as scaffolds for preserving cell shapes. © 2014 Wiley Periodicals, Inc. J. Appl. Polym. Sci. **2015**, *132*, 41801.

KEYWORDS: cell structure; crystal structure; foaming behavior; polypropylene; spherulite

Received 11 August 2014; accepted 23 November 2014

DOI: 10.1002/app.41801

INTRODUCTION

Microcellular plastics are widely used in insulation, packaging, cushion, filters and other fields.[1] In particular, there is much research on the microcellular foam of semi-crystalline polymers due to their heat resistance and mechanical properties. Isotactic polypropylene (iPP) has many desirable and beneficial properties, such as high melting point, high tensile modulus, low density, excellent chemical resistance, and recyclability.[2] These properties of microcellular iPP foam have drawn increasing attention in recent years.

In the approximately two-phase system of PP, the crystallites are nucleated from the melt within a definite temperature range and dispersed in the amorphous matrix. The crystallites grow and aggregate to form birefringent spherulites, which can be observed by optical microscopy under polarized light. In microcellular foaming of amorphous polymers, cells are nucleated homogeneously and the polymer expands uniformly. In solid-state foaming of highly crystallizable polymers, however, absorption and diffusion occur almost exclusively in the amorphous region, and thus, the formed polymer/gas solution is not uniform and the resulting foam structure will be affected by the polymer's crystal morphology.[3] Doroudiani *et al.*[4] observed uniform cells with fine cell size in low-crystallinity polymers while non-uniform structures were developed in high-crystallinity polymers. These phenomena were attributed to the differences of gas solubility and material stiffness in different regions of polymers. The cell density in semi-crystalline polymer was higher than that in amorphous polymer, and thus, the interfaces between the crystalline and amorphous regions could be the preferential cell nucleation sites during the microcellular foaming.[5,6] Microcells were found to appear at the centers and the interlamellar regions of iPP spherulites under relatively low pressure.[7]

To improve the foamability of PP, carbon nanofibers, carbon nanotubes, glass fibers, or wood fibers were added to raise the melt strength and enhance the heterogeneous nucleation during the PP foaming.[8–14] Much more uniform cells and higher mechanical properties were found in PP foam with carbon nanofibers.[15,16] When the added fiber content was high, gradually increased content of carbon fibers led to lower PP crystallinity, higher melt viscoelasticity and higher CO_2 solubility, and finally to more uniform size distribution and higher cell density in the composites.[17,18] The increased cell density was attributed to the heterogeneous cell nucleation with the addition of carbon fibers. The cell structures of PP/wood fiber composites foams were markedly influenced by the length, geometry and content of wood fiber, and higher fiber content resulted in smaller cell size and better physical–mechanical properties.[19]

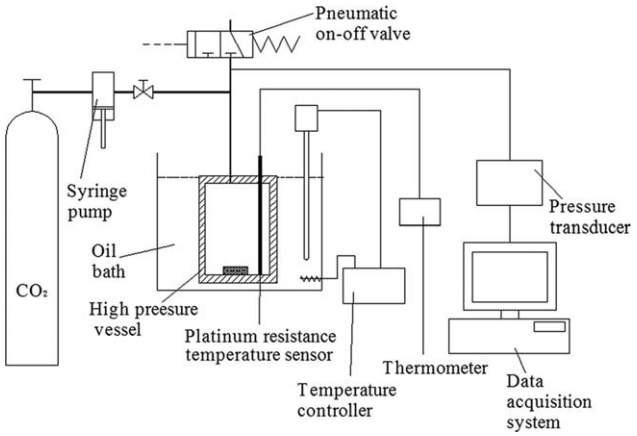

Figure 1. Schematic of the foaming apparatus.

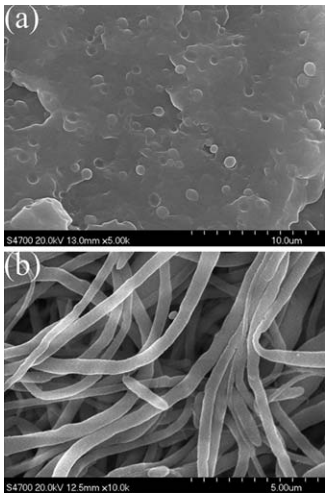

Figure 3. SEM pictures of (a) fractured surface of PP-5sPBT blend and (b) PBT fibers prepared by melt-stretching.

In the past decades, most studies have focused on the foaming of polymer/inorganic fiber composites, but rarely on the foaming of polymer/polymeric fiber composites. In comparison, the polymer/polymeric fiber composites are featured with recyclability, weight reduction, easy processing, and high cost performance.[20] *In situ* microfibrillation of the minor component in PP/polymer system will improve the storage modulus of the blend, and those fibers obviously affect the crystallization of PP.[21] Therefore, all these advantages may be utilized by foaming process. After addition of polytetrafluoroethylene (PTFE) into PP during the foaming, Rizvi *et al.*[22] and Wang *et al.*[23] observed the *in situ* microfibrillation of PTFE, which was due to the shear effect of the screw. The incorporation of microfibrillar PTFE led to increased CO_2 solubility, higher shear storage modulus, and finally to improved foaming behavior of PP. To overcome the drawback of non-uniform cells in iPP foam, therefore, it is necessary to study and compare the foaming behaviors of PP/polymer composites with different shapes of dispersive phases.

In this work, poly(butylenes terephthalate) (PBT) was added into PP to study the foaming behaviors of pure PP, PP/spherical PBT, and PP/fibrous PBT by solid-state foaming. The crystal structures and rheological properties of these composites were used to illustrate the mechanisms behind the special foaming phenomena.

EXPERIMENTAL

Materials

Polymers used in this study included iPP [Sinopec Yangzi Petrochemical, China, PPH-T03-H, melt flow rate (MFR) = 2 g/10 min at 230°C, 2.16 kg], and PBT (Nangtong Xingchen Synthetic Material, China, 1100A, MFR = 23.2 g/10 min at 240°C, 2.16 kg). Melting points of PP and PBT measured by a Q20 differential scanning calorimeter (DSC, TA) were 163 and 225°C, respectively. CO_2 (purity 99%) was purchased from Oxygen Plant, Beijing, China.

Preparation of Sheets of PP and PP/PBT Composites

Prior to melt-mixing, PBT was vacuum-dried at 80°C for 4 h. PP and PBT were mixed (100/0 and 80/20, weight fraction) by a twin-screw extruder (ZSK25-WLE, Werner and Pfleider, Germany) at 240°C with a rotation speed of 100 rpm. Thermal stabilizers were added into the PP/PBT blend to prevent PP from decomposition.

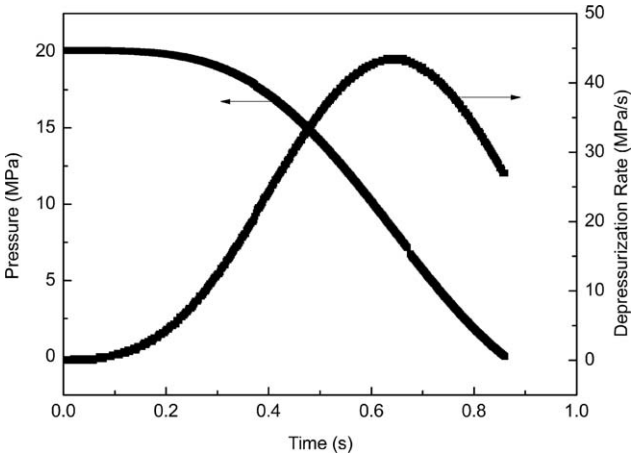

Figure 2. Changes in pressure and depressurization rate with time at a pressure of 20 MPa.

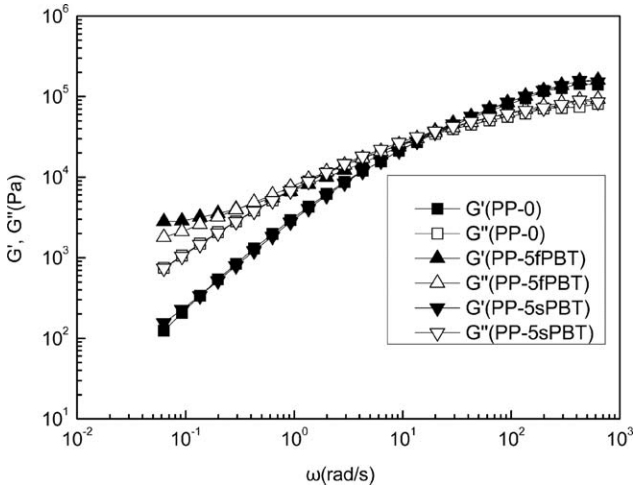

Figure 4. Frequency dependence of oscillatory shear moduli for PP-0, PP-5sPBT, and PP-5fPBT.

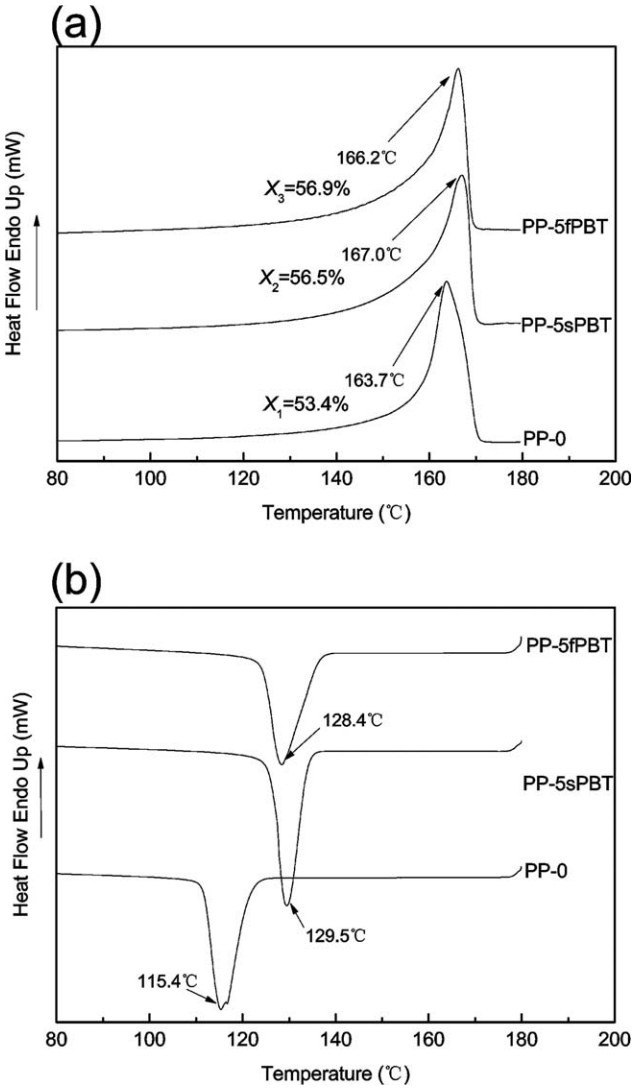

Figure 5. DSC scans of three samples: (a) Melting curves with a heating rate of 5°C min^{-1} and (b) crystallization curves with a cooling rate of 10°C min^{-1}.

To prepare PP composite with spherical PBT, the obtained PP/PBT (80/20) blend was compressed into flat sheets by a laboratory compression-molding machine at 240°C under 10 MPa for 3 min. The sample was then air-cooled.

To prepare PP composite with fibrous PBT, the PP/PBT (80/20) blend was further extruded and melt-stretched by a capillary rheometer (HAAKE Polylab OS, Thermo Fisher Scientific, US) equipped with a rod die (15 mm in length and 1.5 mm in diameter). The die was maintained at 240°C. The stretching was performed by pulling an extruded strand through a set of rollers at a draw ratio of 20. During the stretching, the sample was cooled down immediately.

To dilute the fibers without changing the shape, the stretched strands were blended with pure PP at 190°C, below the melting point of PBT. Mixing was performed in an internal batch mixer at 40 rpm for 3 min. The weight fraction of PBT fibers in the obtained sample was 5%. As a comparison, another PP/PBT (80/20) blend prepared by compression-molding, which had spherical PBT dispersion, was mixed with pure PP at the same conditions to ensure the same thermal history. In this way, the PP/PBT (95/5) blend with spherical PBT was prepared. The pure PP was also prepared in the same conditions. These three types of as-prepared samples with 5 wt % fibrous PBT, 5 wt % spherical PBT and 0 wt % PBT were named as PP-5fPBT, PP-5sPBT, and PP-0, respectively.

These three types of samples were compressed into 1-mm-thick flat sheets by the compression- molding machine at 190°C and 10 MPa for 5 min, and then air-cooled for 10 min to insure the sufficient crystallization of PP.

Foaming Process

Samples of PP-0, PP-5sPBT, and PP-5fPBT were foamed with a depressurization batch foaming apparatus in Figure 1. The central piece of the apparatus was a high pressure vessel with an internal volume of 20 mL. The pressure was measured by a pressure transducer with an accuracy of ±0.1 MPa, and CO_2 was released using a pneumatic on-off valve. A computer installed with an NI data acquisition card was connected to the pressure transducer to record the pressure decay during the depressurization. The internal volume of the high pressure vessel was equally separated by two aluminum sheets into three small cavities, each of which was loaded with a sample (5 × 5 × 1 mm^3, width × length × thickness). The vessel was sealed and immersed in a silicon oil bath to maintain uniform temperature, and its internal temperature was measured by a platinum resistance temperature sensor. After purged with low pressure CO_2, the high pressure vessel was pumped inside with a given amount of CO_2. The CO_2 loading was achieved by a syringe pump. Then the samples were saturated with CO_2 under given pressure and temperature for 3 h, and during this process, the dissolution of CO_2 in PP was balanced. Thereafter, the valve was rapidly opened to release CO_2 in the vessel, and thus, to induce cell nucleation and subsequent growth. Then the vessel was opened quickly, and the foamed samples were taken out for subsequent analyses.

In each of the foaming experiments, the saturation pressure was always fixed at 20 MPa, and the depressurization operations were the same among these experiments with a maximum depressurization rate of about 45 MPa s^{-1}. Figure 2 shows the pressure change during a typical depressurization process. Because the melting point of PP can be reduced by the plasticization of CO_2, the foaming temperature was set below the melting point of PP.[24]

Characterization of Unfoamed Samples

The shapes of dispersive PBT phase before and after stretching were observed by a scanning electron microscope (SEM) (Hitachi S4700). The morphology of PP-5sPBT was examined using a cryogenically fractured sample. Before observation of PBT fibers in PP-5fPBT, the sample was immersed in hot-xylene at 140°C for 2 h to remove PP. The fractured PP-5sPBT blend and the PBT fibers were coated by Pt-Pd prior to the observation.

The rheological properties of these three types of samples were characterized by the frequency dependences of molten-state

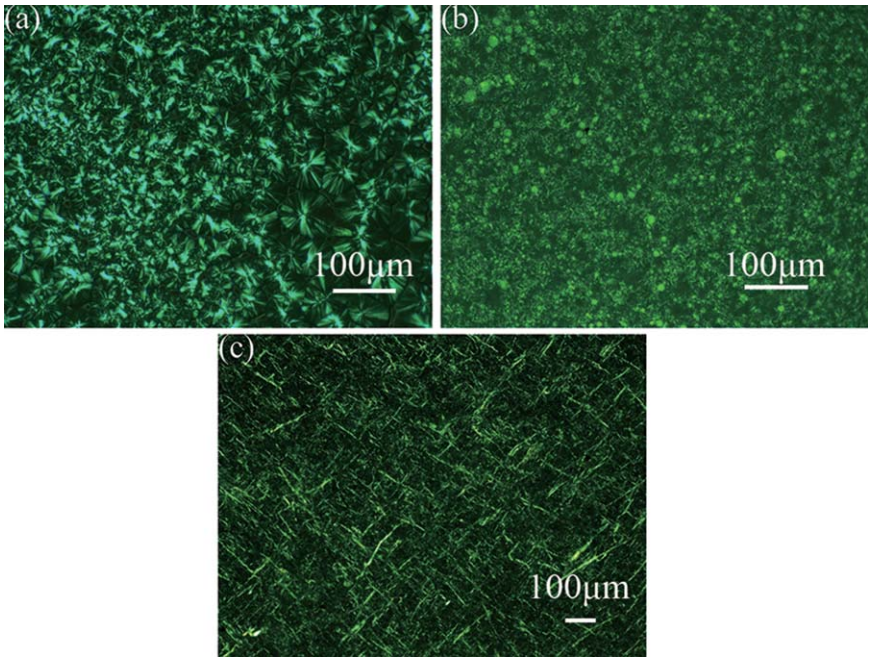

Figure 6. POM pictures of the final crystal morphologies of samples: (a) PP-0, (b) PP-5sPBT, and (c) PP-5fPBT. [Color figure can be viewed in the online issue, which is available at wileyonlinelibrary.com.]

oscillatory shear moduli (e.g., shear storage modulus G' and loss modulus G''), which were evaluated by a parallel-plate rheometer (HAAKE, MARSII) at 190°C in nitrogen atmosphere. The diameter of the plate was 25 mm, and the measure gap was 1 mm.

The crystalline behavior of these three types of unfoamed samples was studied on a DSC. The detailed procedure was set as follows: heat the samples to 180°C at a constant rate of 5°C min^{-1} in nitrogen atmosphere; keep at 180°C for 3 min; cool each sample down to 50°C at a rate of 10°C min^{-1}. The crystallinity, X_c, was estimated as follows:

$$X_c = \frac{\Delta H_m}{\Delta H_{mo} \times \omega} \quad (1)$$

where ΔH_m is the melting enthalpy per gram of a sample, ΔH_{mo} is that of 100% crystalline PP with a constant of 209 J g^{-1},[25] and ω is the weight fraction of PP in the sample.

The crystalline morphology evolutions of PP-0, PP-5sPBT, and PP-5fPBT were observed under a polarized optical microscope (POM) (ZEISS, Axioskop 40) equipped with a hot stage. The tested films were prepared using a laminator at 190°C. To obtain the same crystal structures as these in the unfoamed samples, the hot stage was heated up to 190°C; then kept at 190°C for 3 min to let PP totally melt but maintain the initial shapes of PBT, and finally, the samples were cooled down in the air.

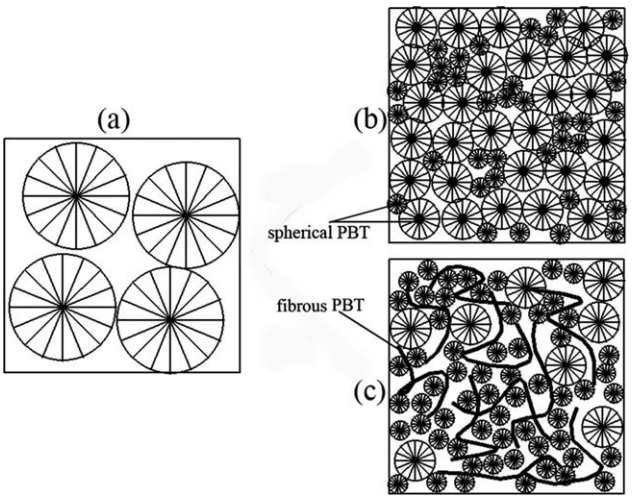

Figure 7. Schematic of the effect of spherical or fibrous PBT on the crystal morphology of PP.

Characterization of Foams

The cell morphologies of foams were characterized by SEM. The foams were immersed in liquid nitrogen for 5 min and then fractured. The fractured surfaces with Pt-Pd coating were scanned with SEM. The average cell size was computed via analysis of SEM photographs on ImageJ software. The number average diameter of all cells in one micrograph, $\bar{d}$, was calculated as follows:

$$\bar{d} = \frac{\sum_{i=1}^{n} d_i}{n} \quad (2)$$

where d_i is the diameter of a single cell, and n is the number of counted cells. At least 100 cells were selected randomly from the SEM graph of each sample to evaluate the average diameter.

The volume expansion ratio of the foamed sample, R_v, was defined as the ratio of the bulk density of the unfoamed one (ρ_0) to that of the foamed one (ρ_f):

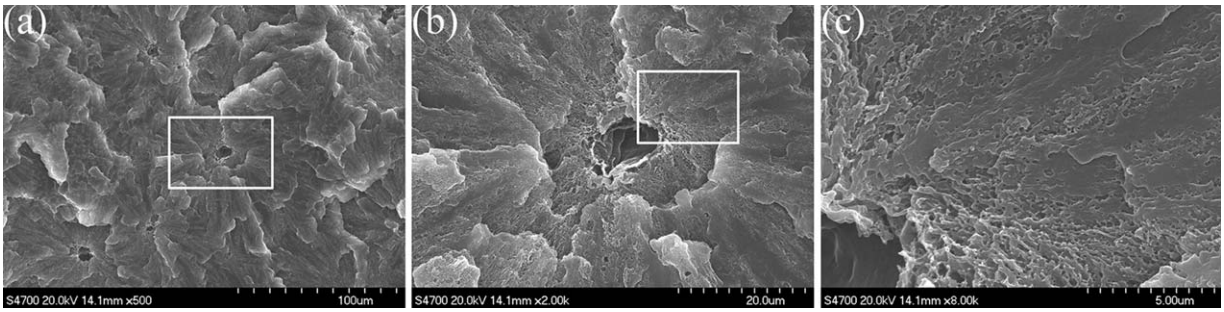

Figure 8. SEM pictures of foamed PP-0 obtained at 152.7°C. (b) magnification of the white rectangle in part (a) and (c) magnification of the white rectangle in part (b).

$$R_v = \frac{\rho_0}{\rho_f} \tag{3}$$

ρ_f was measured according to ASTM D792-00 by weighing polymer foam in water using a sinker. ρ_f was calculated as follows:

$$\rho_f = \frac{a}{a+w-b}\rho_{\text{water}} \tag{4}$$

where a was the apparent mass of a specimen in air without the sinker, b was the apparent mass of the specimen and the sinker completely immersed in water, and w was the apparent mass of the totally immersed sinker.

Porous ratio of the foamed sample, v_f, was defined as the ratio of the volume of gas (v_g) to that of the foam ($v_g + v_p$):

$$v_f = \frac{v_g}{v_g + v_p} \tag{5}$$

The cell density N_0, defined as the number of cells per unit volume of the polymer, was determined as follows:

$$N_0 = \left[\frac{nM^2}{A}\right]^{3/2} R_v \tag{6}$$

where A is the area of an SEM graph (cm^2), n is the number of cells in the micrograph, M is the magnification factor, and R_v is the expansion ratio.

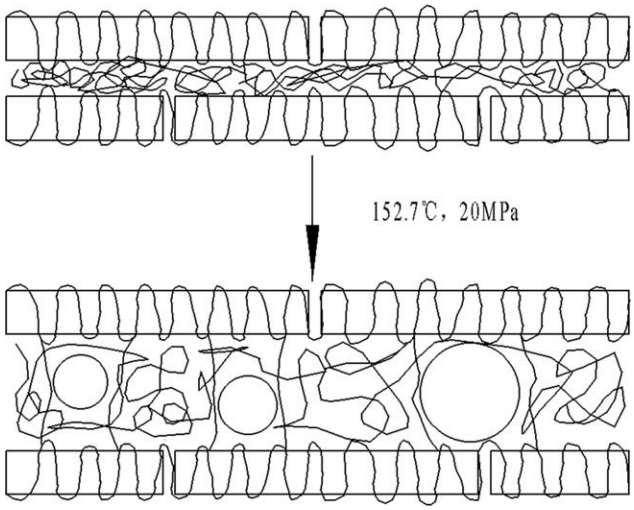

Figure 9. Schematic of cells generated in the interlamellar amorphous regions at a low temperature.

RESULTS AND DISCUSSION

Morphologies of Dispersed PBT

Figure 3(a) shows the fractured surface of PP-5sPBT. The diameters of PBT particles range from 0.3 to 1.2 μm. During the melt-stretching, PBT deformed into a fibrous shape in molten PP as shown in Figure 3(b), in which the PP fraction was totally removed by hot-xylene. The PBT fibers are in diameter of 0.1–1 μm (number average diameter is 0.3 μm), and in length larger than 20 μm, indicating that the aspect ratio is larger than 70. The formation of such long fibers was derived from the coalescence of dispersed droplets by the contraction flow at a die entry and the simple deformation in the melt-stretching. This process is called *in situ* fibrillation.[26]

Rheological Properties of the Blends

Figure 4 shows the frequency dependences of oscillatory shear moduli for PP and PP/PBT at 190°C. The G' curves of PP-0 and PP-5sPBT were close to each other, indicating that spherical PBT did not affect the elasticity of PP; while for PP-5fPBT, the G' was distinctly increased in the low frequency region by the addition of fibrous PBT. The enhanced G' should be owed to the entangled network structure of dispersed fibers. Therefore, frictional force between fibers and bending force of a part of fibers are responsible for the marked elastic property of PP-5fPBT.[27,28]

Melting and Crystalline Behavior of the Blends

The melting and crystalline behavior of PP-0, PP-5sPBT, and PP-5fPBT characterized by DSC are shown in Figure 5. The melting points and crystallinities of PP were slightly raised with the presence of PBT [Figure 5(a)], because solid PBT served as the nuclei of heterogeneous nucleation and promoted the PP crystallization. This heterogeneous nucleation effect can be proved by the substantial increase of onset and peak temperatures during crystallization [Figure 5(b)]. As for the melting point and crystallinity, the PP crystallization was not particularly influenced by the shapes of PBT (spherical or fibrous) during the samples preparation at the same cooling rate.

The POM pictures of the final crystal morphologies of PP-0, PP-5sPBT, and PP-5fPBT are shown in Figure 6. The PP spherulites, with a maximum diameter of larger than 100 μm, are presented as Maltese-cross extinction in Figure 6(a). In the area of high nucleation density, the average diameter of crushed

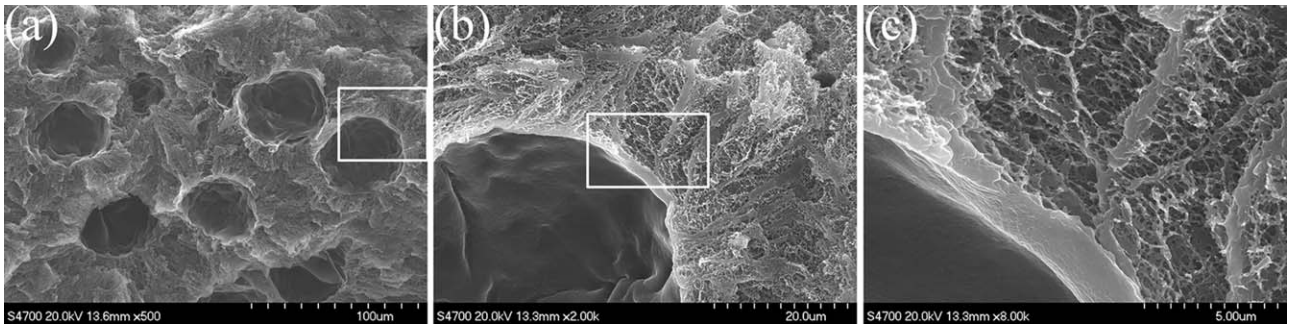

Figure 10. SEM pictures of foamed PP-0 obtained at 154.1°C. (b) magnification of the white rectangle in part (a) and (c) magnification of the white rectangle in part (b).

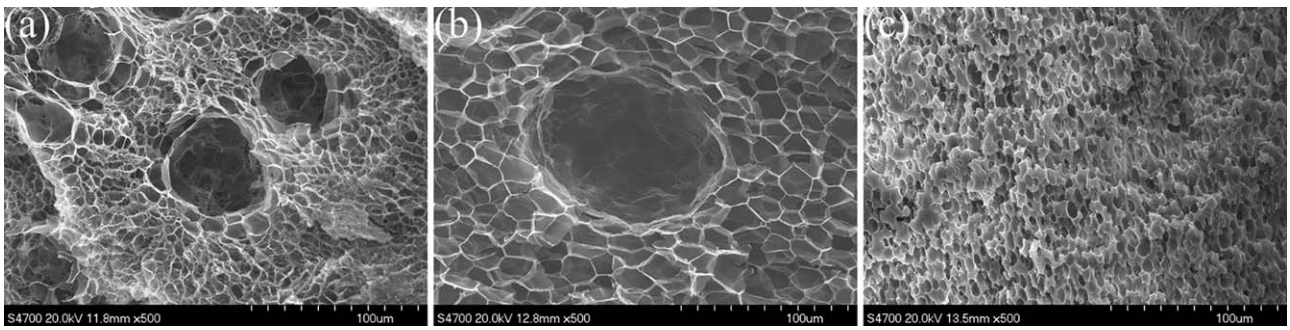

Figure 11. SEM pictures of foamed PP-0 obtained at different temperatures: (a) 155.7°C (b) 157.6°C, and (c) 158.8°C.

Table I. Cell Sizes and Cell Densities of Foamed PP-0, PP-5sPBT, and PP-5fPBT

Temperature	Cell size and cell density	PP-0	PP-5sPBT	PP-5fPBT
152.7°C	$\bar{d}(\mu m)$	8.9	2.9	2.0
	N_O (cells cm^{-3})	2.01×10^6	1.69×10^{10}	8.51×10^9

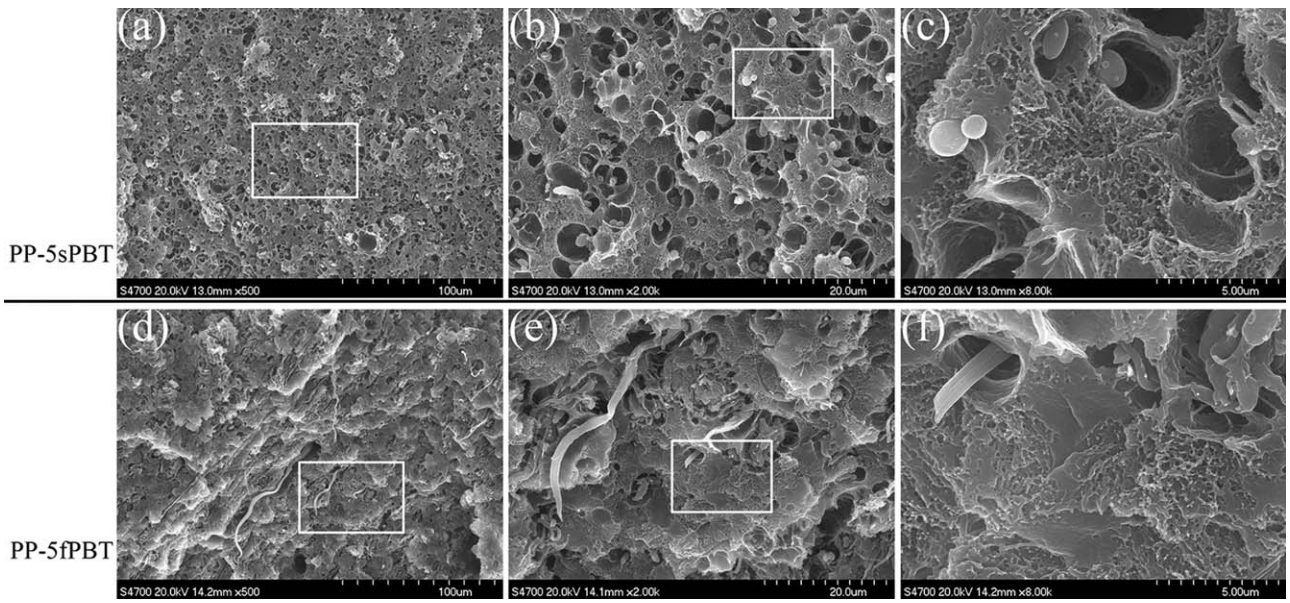

Figure 12. SEM pictures of foamed PP/PBT composites obtained at 152.7°C. (b) magnification of the white rectangle in part (a), (c) magnification of the white rectangle in part (b), (e) magnification of the white rectangle in part (d) and (f) magnification of the white rectangle in part (e).

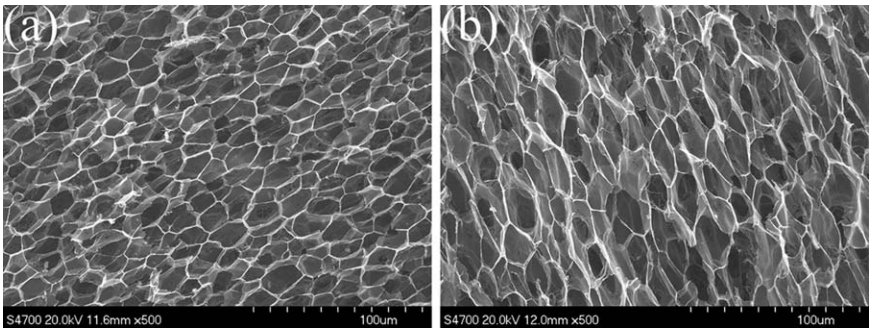

Figure 13. SEM pictures of foamed PP/PBT composites obtained at 155.7°C: (a) PP-5sPBT and (b) PP-5fPBT.

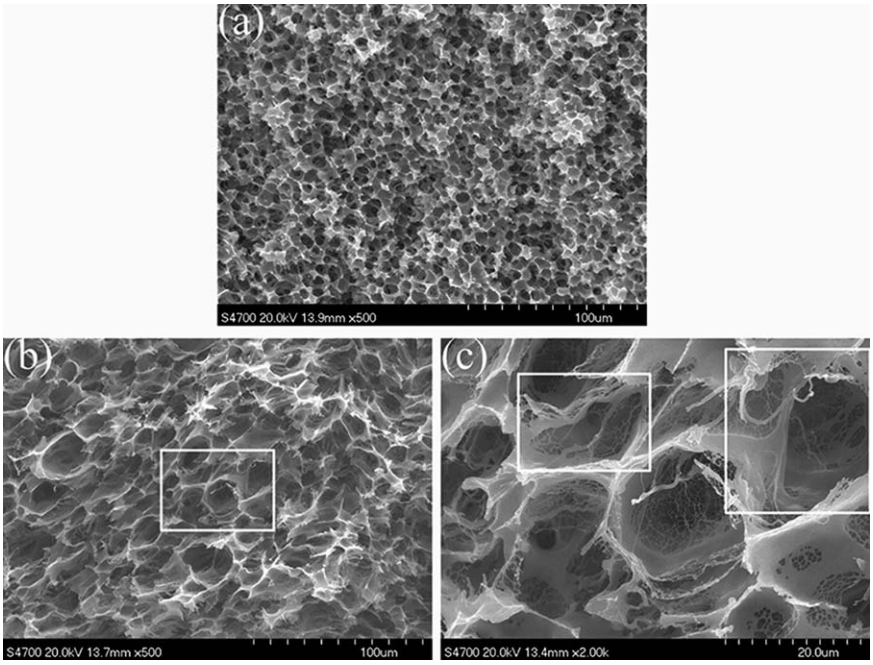

Figure 14. SEM pictures of foamed PP/PBT composites obtained at 157.6°C: (a) PP-5sPBT, (b) PP-5fPBT and (c) magnification of the white rectangle in part (b).

spherulites is about 50 μm. However, the growth space for spherulites was limited by the inducement and disturbance of spherical or fibrous PBT, resulting in the refined spherulites in Figure 6(b,c). The bright circles in Figure 6(b) and the bright lines in Figure 6(c) represent the solid PBT, and the Maltese-crosses among the bright circles or lines display the small spherulites. These results are shown schematically in Figure 7.

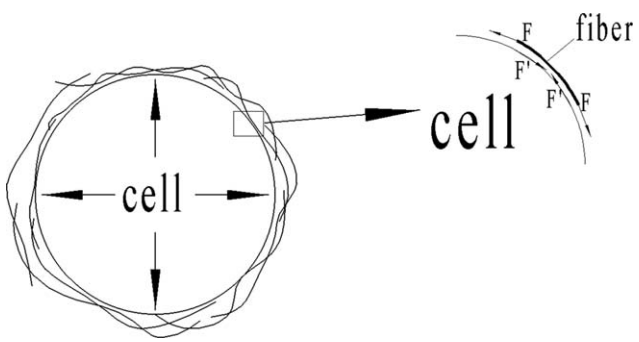

Figure 15. Schematic of cell growth in the foaming of PP-5fPBT.

Effect of Crystal Structure on PP Foaming

Figure 8(a) shows the cell morphology of PP-0 foamed at 152.7°C, and there were only sporadic microcells generated. A higher magnification revealed a number of submicro-sized cells around a microcell [Figure 8(b,c)]. The texture around the microcell was characterized by the radially distributed submicro-sized cells, which revealed the architecture of the corresponding spherulite. The profile of this texture is in size of 50–80 μm, which is consistent with the average size of spherulites in Figure 6(a). We also infer that the microcells were formed from the centers of PP spherulites, and this fact is related to the structural difference between the central area and the dominant radial region in a PP spherulite. In view of those considerations and experimental observations, we believe that under the selected foaming conditions (20 MPa and 152.7°C), the centers of PP spherulites likely begun to melt while the

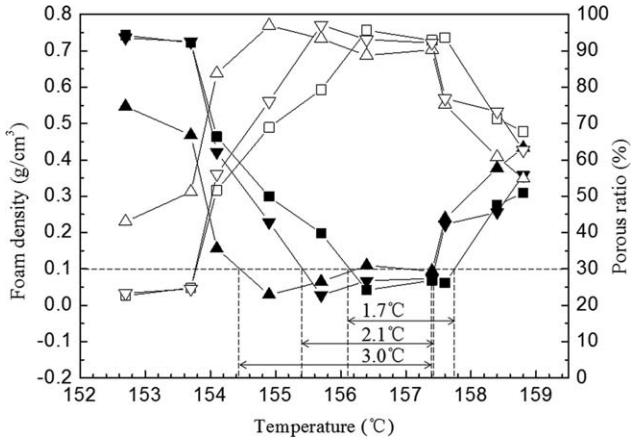

Figure 16. Foam densities (closed symbols) and void fractions (open symbols) of foamed PP-0 (square), PP-5sPBT (upper triangle) and PP-5fPBT (lower triangle).

dominant radial lamellae remained almost unaffected. Once the centers became molten, cells would nucleate and grow there. On the other hand, the radially distributed submicro-sized cells around the microcells indicate that cells could also nucleate in the interlamellar amorphous region, in which CO_2 could be dissolved. However, the cells formed in the interlamellar regions were unable to grow large due to the high viscosity of the lamellae.[7] This conclusion is indicated schematically in Figure 9.

The cell morphology of foamed PP-0 changed significantly at 154.1°C [Figure 10(a)], and it was similar to that obtained at 152.7°C with large cells in the centers of sperulite-like textures. Nevertheless, open cells instead of submicro-sized cells were found in the interlamellar regions [Figure 10(b,c)]. Along with the temperature rise, the centers of spherulites further melted, leading to more severe cell expansion. At the same time, the interlamellar amorphous materials including the thin crystal lamellae were melted. Considering the existence of microcrystals, the high viscosity but low strain at break for PP melt resulted in cell rupture and finally the formation of open cell structure.[29]

The bi-modal cell structure[30] with coexistence of large- and small-cells in foamed PP-0 was still evident at 155.7°C [Figure 11(a)]. The sizes of large-cells obtained by the melting of spherulites even did not change; while the submicro-sized cells around the large-cells grew into microcells. The formation of these microcells resulted from the further decrease of cell growth resistance owing to the further melting of radial lamellae. This bi-modal cell structure still existed at 157.6°C [Figure 11(b)], and did not disappear until 158.8°C [Figure 11(c)].

Different Foaming Behavior of PP/PBT Composites

Compared with PP foam, the cell sizes decreased and cell densities increased significantly in foamed PP/PBT composites [Table I, Figure 12(a,d)]. A higher magnification in Figure 12 revealed that PBT particles and fibers were embedded in microcells surrounded by submicro-sized cells. However, similar radial structure in Figure 8 can hardly be observed here. The formation of these special cell morphologies can be explained by the crystal structure in PP/PBT composites. PP crystallization first occurred at the PP-PBT interface, but the isotropic embryo had highly disordered crystalline arrangement due to the fast crystallization at the early stage. Therefore, the melting occurred around solid PBT, and then cell nucleation and growth took place at the PP-PBT interface [Figure 12(c,f)]. Because the energy barrier of cell nucleation in PP foaming can be reduced by the spherical or fibrous PBT, cells were induced by most PBT particles [Figure 12(b)]. In addition, a cell appeared at the sidewall of the PBT fiber, which was an interesting phenomenon [Figure 12(f)]. Chen *et al.*[31] discovered cell nucleation at the nanotube sidewalls became feasible, and longer nanotubes acted as multiple nucleation sites, leading to an increased cell density. Therefore, this conclusion can also explain the cell formation at the sidewall of PBT fiber. The higher spherulite density was another significant factor that affected the cell densities of PP/PBT composites. At the end stage of PP crystallization, spherulites squashed mutually and their growths were restricted due to higher nucleation density, resulting in the formation of higher-density and smaller-size spherulites.

The heterogeneous nucleation of PBT in PP foaming could be verified by the uniform cells in Figure 13(a,b). Compared with foamed PP-0 obtained at the same temperature [Figure 11(a)], the bi-modal cell structure disappeared and the thin-wall cells became uniform in the foamed PP/PBT composites. As the temperature rose, the foamability gap between the center and the edge of small spherulite was narrowed, so the PP melt was more homogeneous. The homogeneous melt and the heterogeneous cell nucleation of PBT made cells well-distributed.

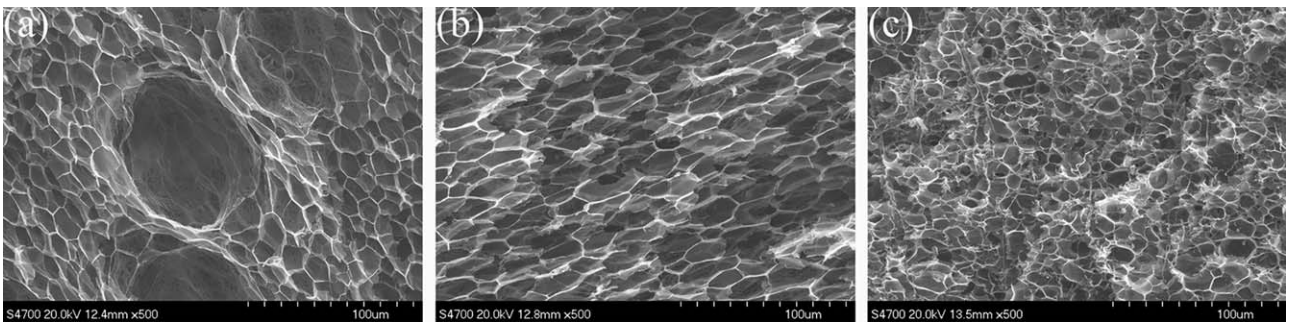

Figure 17. SEM pictures of three foamed samples obtained at 157.4°C: (a) PP-0, (b)PP-5sPBT and (c) PP-5fPBT.

Table II. Cell Sizes and Cell Densities of Foamed PP-0, PP-5sPBT, and PP-5fPBT

Temperature	Cell sizes and cell densities	PP-0	PP-5sPBT	PP-5fPBT
157.4°C	$\bar{d}$ of large-cells (μm)	111	-	-
	N_O of large-cells (cells cm^{-3})	3.41×10^6	-	-
	$\bar{d}$ of small-cells (μm)	15.8	23.3	8.9
	N_O of small-cells (cells cm^{-3})	6.22×10^9	2.01×10^9	1.25×10^{10}

Special Effect of PBT Microfibers on the Foaming of PP/PBT Composites

The temperature of 157.6°C was slightly high for the cells of foamed PP-5sPBT and PP-5fPBT to hold gas during cell expansion, resulting in smaller cell size but thicker cell walls. Nevertheless, there is a significant difference in cell structure between Figure 14(a,b), and their difference in rheological property should be responsible for this. The addition of fibers improved the storage modulus and thus the elasticity of PP-5fPBT at low frequency. In Figure 15, the stretching force F was applied to the fiber around the cell during the expansion; while F', the reacting force of F, reacted on the cell, improving the cell growth resistance. Moreover, the entangled fibers networks served as scaffolds to preserve the cell shapes, which can be proved by the white rectangles in Figure 14(c). The possible mechanism was that entangled fibers network acted in the same way as cytoskeleton in biology. Besides, the PP-5fPBT foam under this condition was rather porous, which might account for its potential of being open-cell foam.

Foam Density and Foaming Temperature Range

The above results indicate that temperature is a vital factor affecting the foaming of PP, so the foaming temperature for preparing foams with fine cell structure must be tailored well. The foam densities of all three types of samples first decreased and then increased as the temperature rose (Figure 16), whereas porous ratios changed in the reversed way. Figure 16 indicates that the temperature range, in which the foam density was lower than 0.1 g cm^{-3}, was about 1.7°C for PP-0, but that was 3.0°C for PP-5sPBT and 2.1°C for PP-5fPBT. In some cases, the temperature range of PP was broadened with the addition of spherical or fibrous PBT. Moreover, the PP/PBT composites showed lower foam densities and higher porous ratios when the temperature was lower than 156.4°C. The cell morphologies and cell parameters of these three types of foamed samples obtained at same temperature of 157.4°C were shown in Figure 17 and Table II, respectively. The bi-modal structure was eliminated and the cells were uniform with the addition of spherical or fibrous PBT. Among them, foamed PP-5fPBT was superior with the smallest cell size and highest cell density.

CONCLUSIONS

The foaming behaviors of PP and PP/PBT composites during solid-state foaming using CO_2 as a blowing agent were investigated. Results show that crystal structure of PP significantly impacted the final cell structure. For pure PP, the melting and foaming first occurred at the centers of spherulites, and then at the radial lamellae regions, leading to the formation of bi-modal cell structure. However, the cell structure was refined with the addition of spherical or fibrous PBT, which could be attributed to the smaller spherulites and heterogeneous cell nucleation with the presence of PBT. The cell growth resistance was increased with the presence of fibrous PBT, which helped to maintain cell shapes.

ACKNOWLEDGMENTS

This work is supported by grant No. 2011BAD24B01 from the 12th National Five-Year Key Technology R&D Program, China.

REFERENCES

1. Klempner, D.; Frisch, K. C. In Handbook of Polymeric Foams and Foam Technology; Hanser: Munich, **1991**; p 17.
2. Vasile, C. In Handbook of Polyolefins; CRC Press: Boca Raton, **2002**; p 267.
3. Sha, H.; Harrison, I. R. *J. Polym. Sci. B Polym. Phys.* **1992**, *30*, 915.
4. Doroudiani, S.; Park, C. B.; Kortschot, M. T. *Polym. Eng. Sci.* **1996**, *36*, 2645.
5. Baldwin, D. F.; Park, C. B.; Suh, N. P. *Polym. Eng. Sci.* **1996**, *36*, 1437.
6. Baldwin, D. F.; Park, C. B.; Suh, N. P. *Polym. Eng. Sci.* **1996**, *36*, 1446.
7. Jiang, X. L.; Liu, T.; Xu, Z. M.; Zhao, L.; Hu, G. H.; Yuan, W. K. *J. Supercrit. Fluids* **2009**, *48*, 167.
8. Selvakumar, P.; Bhatnagar, N. *Mater. Manuf. Process.* **2009**, *24*, 533.
9. Ameli, A.; Nofar, M.; Park, C. B.; Pötschke, P.; Rizvi, G. *Carbon* **2014**, *71*, 206.
10. Chen, C.; Pang, H.; Liu, Z.; Li, Y. B.; Chen, Y. H.; Zhang, W. Q.; Ji, X.; Tang, J. H. *J. Appl. Polym. Sci.* **2013**, *130*, 961.
11. Thompson, M.; Qin, X.; Zhang, G.; Hrymak, A. *J. Appl. Polym. Sci.* **2006**, *102*, 4696.
12. Zheng, G. Q.; Li, Q.; Chen, J. B.; Shen, C. Y.; Yang, W.; Yang, M. B. *Polym. Plast. Technol. Eng.* **2009**, *48*, 170.
13. Rizvi, G. M.; Pop-Iliev, R.; Park, C. B. *J. Cell. Plast.* **2002**, *38*, 367.
14. Zhang, Z. X.; Gao, C.; Xin, Z. X.; Kim, J. K. *Compos. B* **2012**, *43*, 2047.
15. Antunes, M.; Gedler, G.; Velasco, J. I. *J. Cell. Plast.* **2013**, *49*, 259.
16. Antunes, M.; Realinho, V.; Velasco, J. *J. Nanomater* **2010**, *2010*, 1.
17. Wang, C.; Ying, S.; Xiao, Z. *J. Cell. Plast.* **2013**, *49*, 65.
18. Wang, C.; Ying, S. *Fiber. Polym.* **2013**, *14*, 815.

19. Bledzki, A. K.; Faruk, O. *J. Cell. Plast.* **2006**, *42*, 77.
20. Fakirov, S.; Bhattacharyya, D.; Shields, R. *J. Colloids Surf. A* **2008**, 313/314, 2.
21. Shen, J.; Wang, M.; Li, J.; Guo, S. *Polym. Adv. Technol.* **2011**, *22*, 237.
22. Rizvi, A.; Tabatabaei, A.; Barzegari, M. R.; Mahmood, S. H.; Park, C. B. *Polymer* **2013**, *54*, 4645.
23. Wang, K.; Wu, F.; Zhai, W.; Zheng, W. *J. Appl. Polym. Sci.* **2013**, *129*, 2253.
24. Liu, T.; Hu, G. H.; Tong, G. S.; Zhao, L.; Cao, G. P.; Yuan, W. K. *Ind. Eng. Chem. Res.* **2005**, *44*, 4292.
25. Sorrentino, L.; Berardini, F.; Capozzoli, M.; Amitrano, S.; Iannace, S. *J. Appl. Polym. Sci.* **2009**, *113*, 3360.
26. Friedrich, K.; Evstatiev, M.; Fakirov, S.; Evstatiev, O.; Ishii, M.; Harrass, M. *Compos. Sci. Technol.* **2005**, *65*, 107.
27. Yamaguchi, M.; Fukuda, K.; Yokohara, T.; Ali, M. A. B. M.; Nobukawa, S. *Macromol. Mater. Eng.* **2012**, *297*, 654.
28. Yokohara, T.; Nobukawa, S.; Yamaguchi, M. *J. Rheol.* **2011**, *55*, 1205.
29. Li, Y.; Yao, Z.; Chen, Z. H.; Cao, K.; Qiu, S. L.; Zhu, F.; Zeng, C. C.; Huang, Z. M. *Chem. Eng. Sci.* **2011**, *66*, 3656.
30. Bao, J. B.; Liu, T.; Zhao, L.; Hu, G. H. *J. Supercrit. Fluids* **2011**, *55*, 1104.
31. Chen, L. M.; Ozisik, R.; Schadler, L. S. *Polymer* **2010**, *51*, 2368.